Supplemental Material for "Size dependent phase diagrams of Nickel-Carbon nanoparticles"

Y. Magnin,[1] A. Zappelli,[1] H. Amara,[2] F. Ducastelle,[2] and C. Bichara[1]

[1]Centre Interdisciplinaire de Nanoscience de Marseille, Aix-Marseille University and CNRS,
Campus de Luminy, Case 913, F-13288, Marseille, France.
[2]Laboratoire d'Etude des Microstructures, ONERA and CNRS, BP 72, F-92322, Châtillon, France.

Check of the solubility in bulk nickel

Since we will focus on carbon solubility in nanoparticles, we checked that our model correctly reproduces it in bulk systems. Because carbon incorporation in interstitial sites causes an expansion of the system [1], we have to use so-called "osmotic ensemble" Monte Carlo simulations [2]. In our case, the total number of Ni atoms, carbon chemical potential, (zero-) external pressure and temperature are kept constant. Because of the non-trivial atomic interaction model used [3], these calculations are extremely difficult to converge and large hysteresis are observed, starting from either pure solid Ni or C-rich liquid alloy. To get a reasonable order of magnitude of C solubility, very long simulation runs had to be performed, starting from a mixed configuration with a C-rich liquid nucleus inside an essentially solid Ni-C dilute alloy. Only three temperatures of the Ni-C phase diagram could be calculated. We then see in Supp. Mat. Figure 1 that the calculated maximum carbon solubility in solid bulk Ni, is around 5%, in quite good agreement with the experimental one.

Monte Carlo calculation of the carbon sorption isotherms on nickel nanoparticles

The Grand Canonical Monte Carlo algorithm consists here in a series of macro-steps. Each macro-step randomly alternates displacement moves for Ni or C atoms, attempts to incorporate carbon in a previously defined active zone and attempts to remove existing carbon atoms. In order to mimic the CCVD process, the active zone for inserting or extracting carbon atoms is defined as a region of space at less than 0.3 nm above and 0.3 nm below the surface of the Ni cluster. We typically performed up to 5000 macro-steps, but sometimes had to double this number. Within each macro-step, we systematically achieved four times the number of atom attempted displacement steps. To incorporate (resp. remove) carbon atoms in the structure, 1000 attempts were made and the corresponding routine was exited as soon as the first successful incorporation (resp. deletion) occurred. We usually started from pristine crystalline Ni NPs, but checked that the result was stable against a change of the initial configuration. We also checked that the amount of C adsorbed did not significantly depend on the choice of the thickness of the incorporation active zone, at least for the smallest NP sizes. Because of the large surface/bulk ratio, hysteresis problems are less critical than in the bulk. However, calculations turn out to be extremely long for the biggest NPs (up to 3 months for 807 Ni atoms and large fractions of C incorporated). This might lead to systematic underestimation of the C fractions. For smaller NPs fluctuations are more important, leading to some statistical noise, especially in the case of core / shell NPs.

Once the equilibrium is reached, the number of C incorporated in the NP fluctuates around an average value. We record the number of C atoms adsorbed inside the cluster at given μ_C and T. Quite obviously, once the NP is saturated with carbon, for high values of μ_C, C atoms are also stabilized on the surface or outside the NP. We do not consider them in the present study. In Supp. Mat. Figure 2, we present the C sorption isotherms at 4 temperatures: 680, 850, 1020 and 1190 K. Some of the already published data [4] are presented here for the sake of completeness. New calculations include the icosahedral NP with 309 Ni atoms. The convergence of the runs with 405 and 807 was also improved.

Analysis of the solid / liquid state of the nanoparticles

The atomic structure of the nanoparticles is then investigated using the local order parameter (S_i) proposed by Steinhardt et al. [5], and improved by Jungblut et al. [6], equation (1), to define the ordered or disordered (i.e.: amorphous or liquid) parts of the nanoparticles. This parameter reflects the symmetry of the local environment of each atom, making use of spherical harmonics. It writes:

$$S_i = \frac{1}{N_b} \sum_{j=1}^{N_b} \frac{\sum_{m=-6}^{6} q_{6m}(i) q_{6m}^*(j)}{\left(\sum_{m=-6}^{6} |q_{6m}(i)|^2 \right)^{1/2} \left(\sum_{m=-6}^{6} |q_{6m}(j)|^2 \right)^{1/2}} \quad (1)$$

where N_b is the number of neighbors j of atom i,

$$q_{6m}(i) \; = \; \frac{1}{N(i)} \sum_{j=1}^{N(i)} Y_{6m}\left(\theta(\mathbf{r}_{ij}), \phi(\mathbf{r}_{ij})\right) \tag{2}$$

and Y_{lm} is the spherical harmonic of degree l and order m.

Averaging over the Ni atoms of the NP yields a global order parameter $\bar{S}$, used in the following to establish the phase diagram. $\bar{S}$ is normalized in such a way that a perfectly crystallized structure has $\bar{S}$=1, while a fully disordered structure corresponds to $\bar{S}$=0. These are limiting values and we practically consider structures with $\bar{S} \geq 0.85$ as solid and those with $\bar{S} \leq 0.35$ as liquid.

Phase diagram calculation

The first step is to plot the global order parameter ($\bar{S}$) as a function of μ_C, at different temperatures. A typical result is presented in Supp. Mat. Figure 3 that presents the transition from a crystalline NP, with $\bar{S} \sim 0.95$ for $\mu_C \leq$ -7.0 eV/atom to a disordered one, with $\bar{S} \leq 0.30$ for $\mu_C \geq$ -6.2 eV/atom. In the intermediate region (-7.0 $\leq \mu_C \leq$ -6.2 eV/atom), we note that $\bar{S}$ depends linearly on μ_C. This is a characteristic feature of the "phase transition" in a nano-sized system that continuously evolves from solid to liquid by forming liquid shell / solid core nanoparticles. In a large bulk system, the solid / liquid transition would take place at a fixed μ_C value. The intersections of the three pieces of straight lines yield the carbon chemical potentials at the transition points that are readily translated in carbon concentration using the carbon sorption isotherm. The corresponding solid and liquid points are then reported on the phase diagram. This procedure is repeated at different temperatures and for different nanoparticle sizes to obtain the solvus and liquidus lines of the phase diagrams.

Detailed presentation of the phase diagram for 807 nickel nanoparticle

In order to better understand how the phase diagrams were built, we provide more visual information on the structure of the nanoparticles with 807 Ni atoms and different carbon fractions. Results are shown in Supp. Mat. Figure 4, that presents 16 snapshots of NPs at different locations in the (x_C, T) phase diagram. In particular, along the M, I, E and A configurations that contain $\sim$ 8% C at temperatures between 1200 and 700 K, we see a continuous evolution in the core shell structures, without any significant change at the eutectic temperature. This supports the idea that the liquid C-saturation line can be extrapolated below the eutectic temperature and, consequently, that no 3 phase equilibrium line exists in small NPs.

Formation energy of carbon interstitials in icosahedral nanoparticles

Table I displays the formation energy of carbon inserted in subsurface interstitial sites of I_h nanoparticles with 55, 147 and 309 Ni atoms. They are calculated according to the formula: $\Delta E = E_{NP+1C} - E_{NP} - E_C$. E_C is the energy of a carbon atom in a graphene layer, taken as a reference. The energies of the clusters are extrapolated to 0 K, after a simulated annealing between 300 and 10 K. The error bars on the energies result from this linear fitting procedure. I_h NPs present triangular facets with a number of non-equivalent subsurface sites identified by numbers 1 to 5 in Supp. Mat. Figure 5. After relaxation, all sites are distorted. The strain is calculated by averaging the differences of the 4 or 6 distances between the center of the interstitial cavity and the first neighbors [7], after and before relaxation. We can see that:

1. For a given size, octahedral sites are more stable than tetrahedral ones;

2. Carbon incorporation is more favorable in smaller size clusters;

3. For the Ni$_{309}$ NP, and probably also for larger ones, icosahedral interstitials become unstable while octahedral ones tend towards the bulk value presented in [1];

4. As expected because they are smaller, icosahedral interstitial sites are more strained than octahedral ones after relaxation.
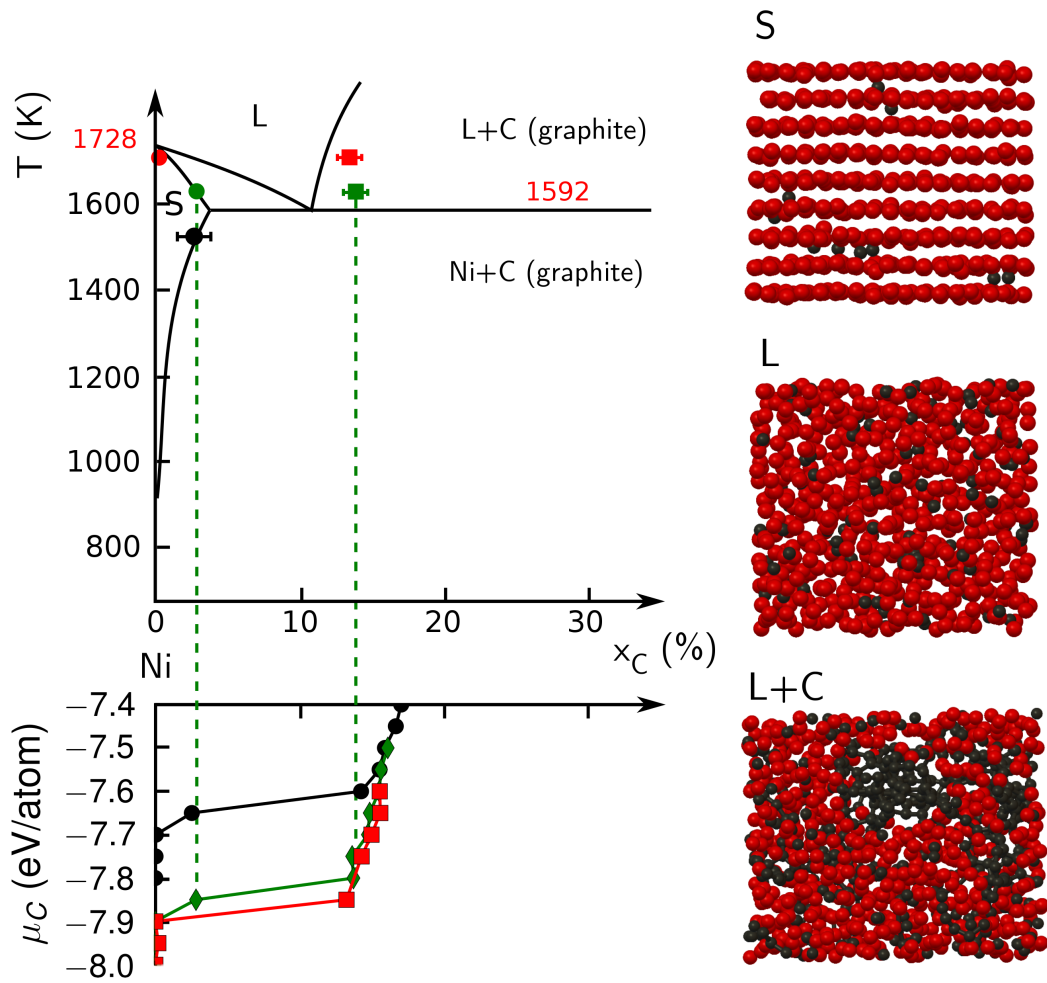
FIG. 1: (Color online) Carbon incorporation isotherms in a 576 Ni bulk system (lower figure) and the corresponding phase boundary points of the phase diagrams, compared to the experimental one [8] (full black lines, upper figure). The red, green and black circles on the phase diagram correspond to the carbon solubility limit in the solid at 1700, 1615 and 1530 K respectively. The red and green squares indicate the C concentration in the liquid, at the next carbon chemical potential step, 0.05 eV/atom higher. Calculations at 1530 K and -7.60 eV/atom did not show a convergence of the C concentration, but the simulation box was clearly disordered: this is the reason why it is not shown on the phase diagram. Three typical situations (solid with C dissolved, homogenous liquid and carbon segregation from the liquid) are depicted on the right.
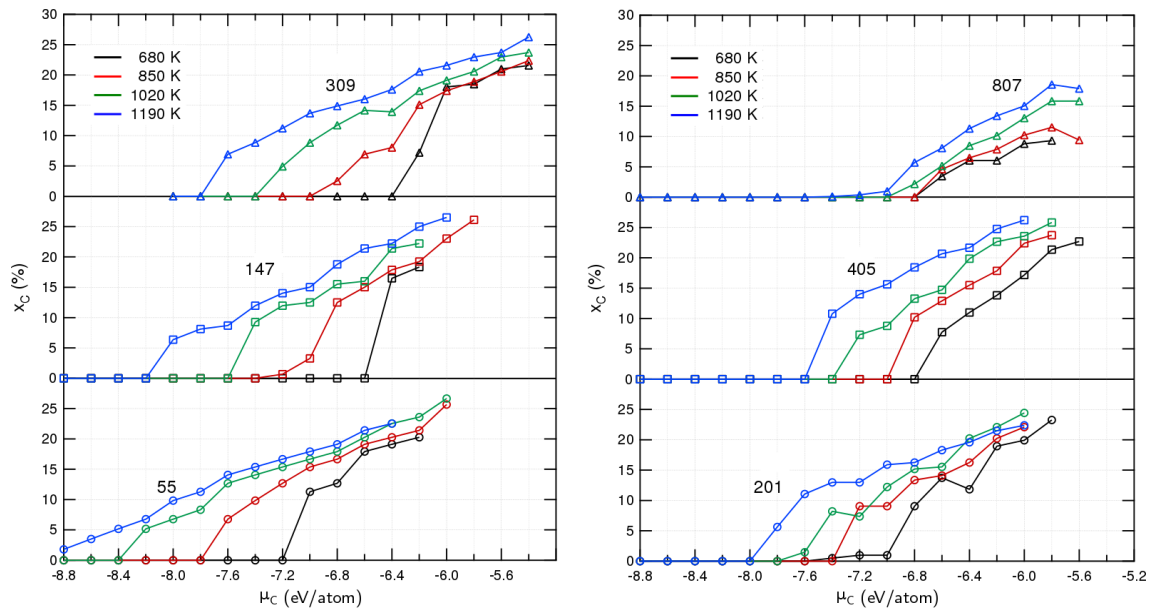
FIG. 2: (Color online) Carbon sorption isotherms on icosahedral (left), with 55, 147 and 309 Ni atoms, and face centered cubic, Wulff shaped (right), with 201, 405, 807 Ni atoms nanoparticles. These curves present the carbon fraction (x_C) inside the nanoparticle, as a function of temperature and C chemical potential (μ_C). Low values of μ_C, lead to a small fraction of C dissolved. Increasing μ_C, the C fraction (x_C) continuously grows, while the NP gradually melts. At constant μ_C, the fraction of dissolved C is larger at higher temperatures.
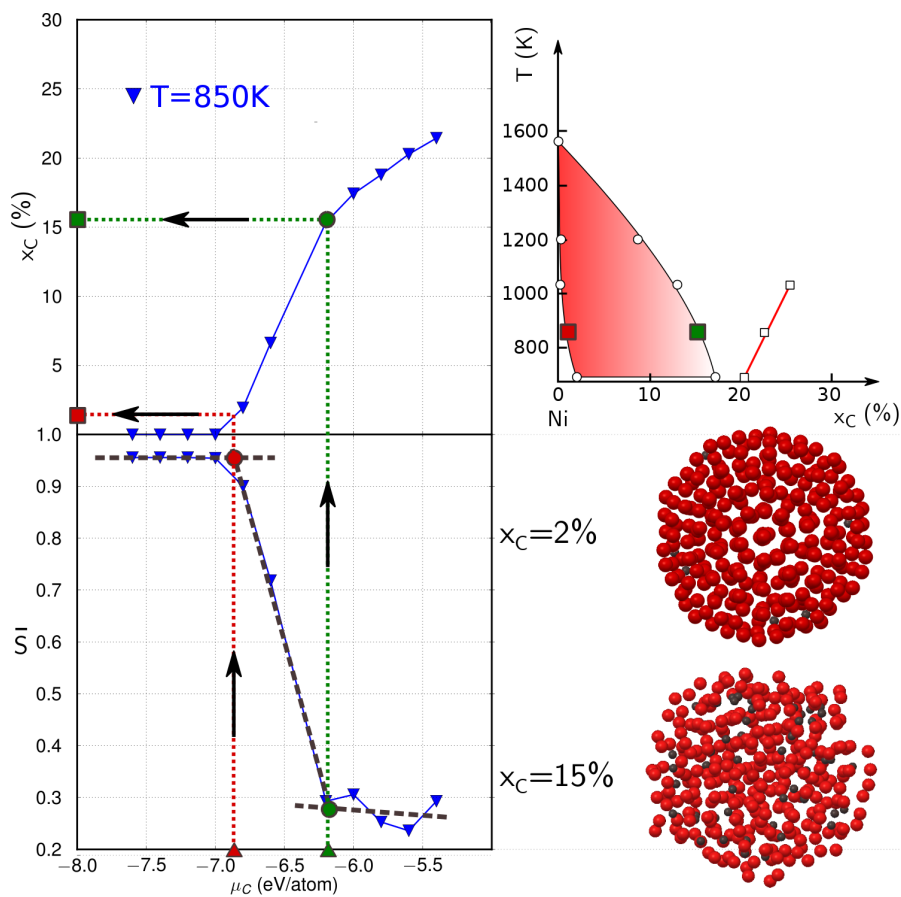
FIG. 3: (Color online) Determination of phase boundaries of an icosahedral particle with 309 Ni atoms. The liquid ($\bar{S} < 0.35$) and solid ($\bar{S} > 0.90$) boundaries are determined in the ($\bar{S}$, μ_C) plane (lower panel) and the corresponding concentrations are then obtained from the C incorporation isotherm (upper panel) and located in the phase diagram.
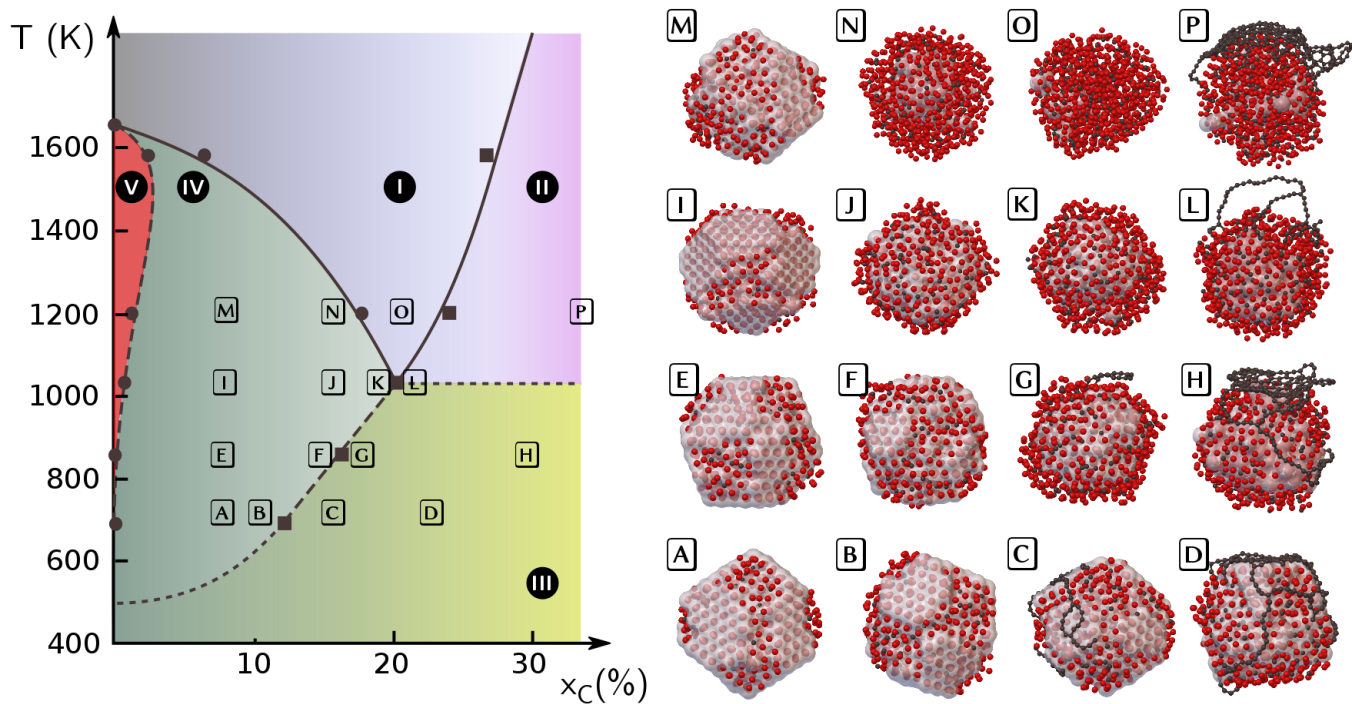
FIG. 4: (Color online) Left panel: Ni-C phase diagram for a nanoparticle with 807 Ni atoms.
The red domain (V), limited by a dashed solvus line, corresponds to a homogenous solid solution. The blue domain (I), limited by liquidus lines (full), corresponds to homogenous liquid NPs. The left green region (IV), between V and I, corresponds to solid core / liquid shell nanoparticles. On the right of the phase diagram, a segregation of carbon at the surface of the NP is observed, on liquid (purple, II) or core / shell (yellow green, III) nanoparticles. The dashed line separating domains III and IV at temperatures below 700 K is hypothetical, while the dashed line between 700 and 1000 K, is an extrapolation of the solubility limit into the core / shell domain, supported by an analysis of the atomic configurations. Right panel: images of the NPs located in the left panel phase diagram by the position of their identification letter. The grey surface is a contour of the solid core of the NP, if it exists. Red and black balls respectively correspond to Ni atoms with a small $\bar{S} >$ parameter ("liquid") and their surrounding C atoms.

Site	$I_h 55$	Number of sites	$I_h 147$	Number of sites	$I_h 309$	Number of sites
Tetrahedron	$\Delta E_1 = -0.81 \pm 0.01$ eV	3	$\Delta E_1 = -0.47 \pm 0.02$ eV	3	$\Delta E_1 = -0.18 \pm 0.03$ eV	3
			$\Delta E_3 = -0.58 \pm 0.02$ eV	3	$\Delta E_3 = 0.15 \pm 0.03$ eV	6
					$\Delta E_4 = 1.94 \pm 0.03$ eV	1
Octahedron	$\Delta E_2 = -1.73 \pm 0.01$ eV	1	$\Delta E_2 = -0.62 \pm 0.02$ eV	3	$\Delta E_2 = -0.40 \pm 0.03$ eV	3
					$\Delta E_5 = -0.20 \pm 0.03$ eV	3
Tetrahedron	$\epsilon_1 = 28\%$	3	$\epsilon_1 = 25\%$	3	$\epsilon_1 = 19\%$	3
			$\epsilon_3 = 28\%$	3	$\epsilon_3 = 19\%$	6
					$\epsilon_4 = 20\%$	1
Octahedron	$\epsilon_2 = 5\%$	1	$\epsilon_2 = 3\%$	3	$\epsilon_2 = 6\%$	3
					$\epsilon_5 = 6\%$	3

TABLE I: Formation energy and strain of carbon inserted in subsurface interstitial sites of I_h nanoparticles with 55, 147 and 309 Ni atoms. Energy and strain indexes correspond to the locations of carbon insertion, as depicted in Supp. Mat. Figure 5.
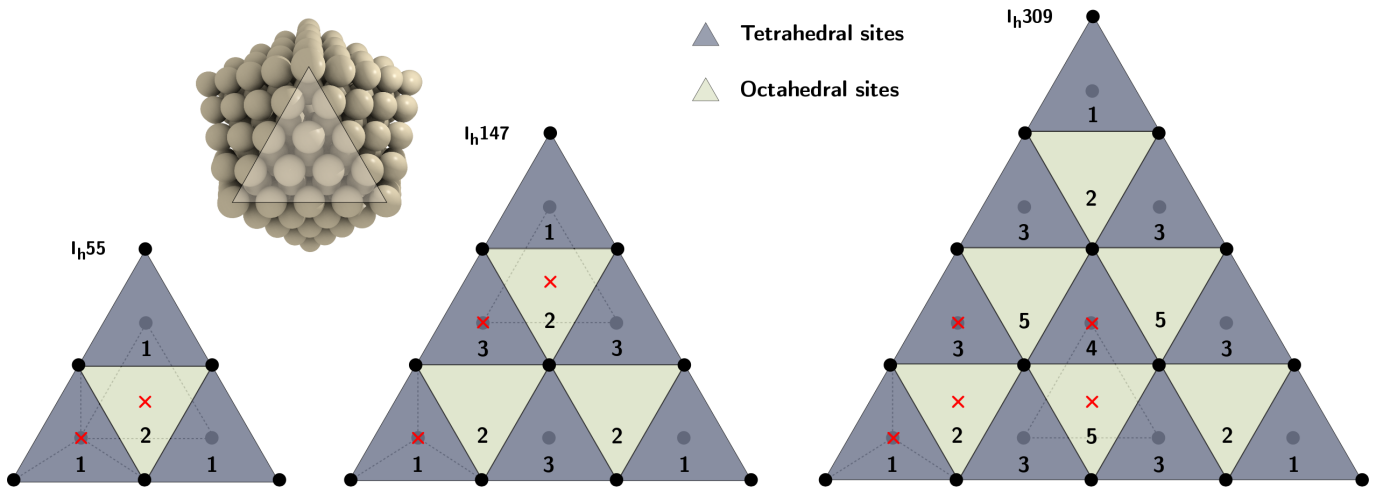

FIG. 5: Representation of I_h (111) facets of NPs with 55, 147 and 309 Ni atoms. Red crosses indicate the carbon interstitial sites, located below the corresponding triangles. Dark (resp. light) triangles correspond to tetrahedral (resp. octahedral) sites.

[1] M. Moors, H. Amara, T. Visart De Bocarmé,C. Bichara, F. Ducastelle, N. Kruse, J.-C. Charlier, ACS Nano, **3**, 511 (2009).
[2] F.-X. Coudert, M. Jeffroy, A. H. Fuchs, A. Boutin, C. Mellot-Draznieks, J. Am. Chem. Soc., **130**, 14294 (2008).
[3] H. Amara, J.-M. Roussel, C. Bichara, J.-P. Gaspard and F. Ducastelle, Phys. Rev. B, **79**, 014109 (2009).
[4] M. Diarra, H. Amara, F. Ducastelle and C. Bichara, Phys. Status Solidi, **249**, 2629 (2012).
[5] P. Steinhardt, D. Nelson, M. Ronchetti, Phys. Rev. B, **28**, 784 (1983).
[6] S. Jungblut, A. Singraber, C. Dellago, Mol. Phys., **111**, 3527 (2013).
[7] S. Li, M. S. Sellers, C. Basaran, A. J. Schultz, D. A. Kofke, Int. J. Mol. Sci., **10**, 2798 (2009).
[8] V. K. Portnoi, A. V. Leonov, S. N. Mudretsova and S. A. Fedotov, Phys. Met. Metallogr., **109**, 153 (2010).